(angiogenesis).[5] As these nascent vessels only consist of endothelial cells, they rupture easily and are leaky, prone to regression, and poorly perfused.[18,20–22] Recruitment of mural cells around nascent vessels essentially contributes to remodeling and maturation of the primitive vascular network (arteriogenesis), subsequently causing therapeutic improvement of blood perfusion.[5,18] We found a larger percentage of vessels without lectin staining and lower maturation index in the control and single treatment groups, indicating that promotion of angiogenesis, but failure to effectively induce arteriogenesis. Consequently, the single treatments showed only transient effects on global cardiac function and limited functional capacity, possibly due to irregular capillary networks and increased vascular permeability. In the combined treatment group, greater numbers of functionally and structurally mature vessels were established promptly after treatment and maintained in ischemic myocardium. This might be primarily attributed to upregulated expressions of genes related to angiogenesis (*VEGF, VEGFR-1, VEGF-R2, Akt-1*) and/or endogenous regeneration (*SDF-1*). Moreover, elevated expressions of *Ang-1* and its receptor *Tie-2*, and *PDGF, VE-cadherin*, and *PECAM* might play key roles in promoting maturation processes such as "stabilization" of cell junctions and tight pericyte recruitment (arteriogenesis).[5,15,16,18,20–22] Interestingly, the elevated expression of the those relevant genes shown in the combined group was mostly reduced after 28 days after treatment (data not shown), corresponding with reduced donor cell presence. We found, however, the combined treatment group showed more sustained positive effects on vessel maturity and cardiac function recovery as compared with the control and single treatment groups at 28 days after treatment, indicating that paracrine mediators contribute to the myocardial recovery mainly during the early phase after the treatment and the effects on cardiac function and vessel structure, once established, could last for a longer time.[2] These data suggest that OM-flap covering the cell-sheet played a key role in accomplishing the maturity of the new vessels in the targeted myocardial territory, leading to formation of more organized and durable vascular network, as compared to the control and the single treatment groups.

Endothelial vasodilator function of coronary microvessels (resistance arterial vessels) is an important determinant of myocardial perfusion in response to increased myocardial oxygen demand, playing a critical role in neovascular therapies.[6–8] Vasodilation in response to specific endothelium-dependent and endothelium-independent stimuli within the coronary circulations can be measured to assess endothelial function. To the best of our knowledge, this is the first to verify that cell-sheet treatment with and without OM-flap could improve endothelial vasodilator function of resistance arterial vessels in a rat MI model, utilizing *in vivo* synchrotron-based microangiography that has proved an effective method for clearly visualizing resistance arterioles and accurately identifying neurohumoral modulation of coronary blood flow within the microcirculation for assessing therapy efficacy.[7,23,24] Microangiography revealed attenuated dilatation and a strong trend toward increased incidence of paradoxical constrictions in the control, followed by the single treatment group, suggesting that the endothelial-dependent vasodilator function in resistance arterial vessels was progressively impaired in those groups.[25,26] In contrast, combined treatment effectively restored endothelial function in resistance arterial vessels, evidenced by better dilatory responses to acetylcholine, an endothelium-dependent vasodilator.[27] This corresponds with PET/CT findings demonstrating substantial improvement in CFR, which indicated the ability of the myocardium to increase blood flow in response to increasing myocardial oxygen demand. Adenosine causes vasodilation by stimulating receptors in the microcirculation, facilitating measurement of the endothelium-independent CFR in the microcirculation. Interestingly, a remarkable improvement in CFR was observed in basal, but not apical LV, indicating that the combined treatment might be capable of improving microvasculature functionality of hibernating myocardium, rather than scar cardiac tissue. These physiological benefits in the coronary microcirculation may activate collateral growth through increased flow and shear stress, a powerful driving force of arteriogenesis, leading to enhanced functional capacity under a high load.[28,29] Therefore, we speculate that the present combined treatment strategy has potential to effectively prevent progression of endothelial dysfunction, which independently predicts major clinical adverse events in patients with heart failure.[28–30]

Our data suggest that the combination of cell sheet transplantation and OM-flap acts synergistically, rather than additively, on vessel maturation, coronary microcirculation physiology, functional capacity, and cardiac reverse remodeling, whereas the OM-only strategy failed to stabilize its long-term effect. These results encouraged us to investigate the role of the cell-sheet transplantation in activating the effects of OM-flap. Postmortem angiography findings demonstrated visible collateral vessels between the native coronary arteries and OM-flap in the combined group, whereas no tight junctions were shown in the OM-only group, indicating that formation of collateral vessels between native coronary arteries and OM was accelerated by the interposed cell-sheets. The possible mechanism of those findings might be explained by our *in vitro* migration assay demonstrating that growth factors and cytokines secreted by the cell-sheet stimulate migration of endothelial cells derived from both host myocardium and the OM toward the sheet, subsequently establishing robust vessel connections with persistent blood flow between the native coronary arteries and OM. In contrast, in the OM-only group, lack of that process caused immature leaky collateral vessel formation and thus inadequate collateral blood flow in the ischemic myocardium. Based on those findings, we speculate that the therapeutic effects of the combined treatment strategy might be responsible for increased donor cell survival and stimulation of donor cells induced by OM-flap as well as for cell-sheet–mediated activation of OM-flap as a donor artery with high perfusion capacity. Nevertheless, further studies are absolutely needed to determine the main molecular mechanism of therapeutic effects induced by the combined treatment.

LIMITATIONS

Considering the potential molecular mechanisms behind the beneficial histological and physiological alterations observed with the combined strategy, we found that a group of possibly relevant molecules including *VEGF-A*, *VEGF receptor-1*, *VEGF receptor-2*, *Akt-1*, *SDF-1*, *PDGF-β*, *Ang-1*, *Tie-2*, *VE-cadherin*, and *PECAM* were upregulated in the combined group, suggesting that the

effects may be attributed to activation of several paracrine molecules, rather than a single molecule. Although some may argue what kinds of cytokines play a major role in generating therapeutic effects among the many complex molecular and cellular mechanisms involved, we consider that establishment of mature vessels is a complex process that is not regulated by specific factors, but rather numerous multiple factors that also dynamically change in response to the process of angiogenesis or vessel maturation. We believe that use of a cell-sheet and pedicle-OM as synergistic intelligent engineered tissues can efficiently support the regenerative process by dynamic cross-talk with ischemic cardiac tissue.

Although we did not experience any complication such as torsion of omentum flap or diaphragmatic hernia in the rats receiving the combined treatment, it is considered that a conventional lapalotomy itself may adversely affect general conditions particularly in critically-ill heart failure patients. An endoscopic approach may be useful in minimizing the OM-flap procedure-related complications in clinical settings.

CONCLUSION

We demonstrated that cell-sheet transplantation with an omentum-flap better promoted arteriogenesis and improved coronary microcirculation physiology in ischemic myocardium tissue, leading to potent functional recovery in a rat MI model. Further development of this treatment strategy toward clinical application is encouraged.

MATERIALS AND METHODS

All experimental procedures were approved by an institutional ethics committee. Animal care was conducted humanely in compliance with the Principles of Laboratory Animal Care formulated by the National Society for Medical Research and the Guide for the Care and Use of Laboratory Animals, prepared by the Institute of Animal Resources and published by the National Institutes of Health (publication no. 85-23, revised 1996).

Two weeks after left coronary artery ligation, rats were divided into four groups: (i) skeletal myoblast cell-sheet transplantation covered with an OM-flap (combined group), (ii) cell-sheet transplantation only, (iii) OM-flap only, and (iv) sham operation (control group). The protocol of this study is shown in **Figure 1a,b**. All *in vivo* and *in vitro* assessments were carried out in a blinded manner. A detailed description of all methods and reagents used for the experiments is provided in the **Supplementary Materials and Methods**.

SUPPLEMENTARY MATERIAL

Figure S1. Frequency distribution charts showing individual segment caliber changes in response to acetylcholine in **(a)** third and **(b)** fourth branching order vessels.
Materials and Methods.

ACKNOWLEDGMENTS

We thank Tsuyoshi Ishikawa, Yuuka Fujiwara, Yuka Kataoka, Hiromi Nishinaka, Toshika Senba, and staff of the PET Molecular Imaging Center for their excellent technical assistance. This research was supported by Research on Regenerative Medicine for Clinical Application from the Ministry of Health, Labour and Welfare of Japan and the Australian Synchrotron International Synchrotron Access Program (ISAP AS-IA111). Experiments were performed at the Japan Synchrotron Radiation Research Institute (SPring-8, BL28B2, Proposal 2011A1169). T.S. is a consultant for CellSeed, Inc., and T.O. is an Advisory Board Member of CellSeed, Inc. and an inventor/developer holding a patent for temperature-responsive culture surfaces. The authors have no conflicts of interest to report.

REFERENCES

1. Shah, AM and Mann, DL (2011). In search of new therapeutic targets and strategies for heart failure: recent advances in basic science. *Lancet* **378**: 704–712.
2. Narita, T, Shintani, Y, Ikebe, C, Kaneko, M, Harada, N, Tshuma, N *et al.* (2013). The use of cell-sheet technique eliminates arrhythmogenicity of skeletal myoblast-based therapy to the heart with enhanced therapeutic effects. *Int J Cardiol* **168**: 261–269.
3. Sekiya, N, Matsumiya, G, Miyagawa, S, Saito, A, Shimizu, T, Okano, T *et al.* (2009). Layered implantation of myoblast sheets attenuates adverse cardiac remodeling of the infarcted heart. *J Thorac Cardiovasc Surg* **138**: 985–993.
4. Habib, GB, Heibig, J, Forman, SA, Brown, BG, Roberts, R, Terrin, ML *et al.* (1991). Influence of coronary collateral vessels on myocardial infarct size in humans. Results of phase I thrombolysis in myocardial infarction (TIMI) trial. The TIMI Investigators. *Circulation* **83**: 739–746.
5. Carmeliet, P and Jain, RK (2011). Molecular mechanisms and clinical applications of angiogenesis. *Nature* **473**: 298–307.
6. Gutiérrez, E, Flammer, AJ, Lerman, LO, Elízaga, J, Lerman, A and Fernández-Avilés, F (2013). Endothelial dysfunction over the course of coronary artery disease. *Eur Heart J* **34**: 3175–3181.
7. Shirai, M, Schwenke, DO, Tsuchimochi, H, Umetani, K, Yagi, N and Pearson, JT (2013). Synchrotron radiation imaging for advancing our understanding of cardiovascular function. *Circ Res* **112**: 209–221.
8. Furchgott, RF and Zawadzki, JV (1980). The obligatory role of endothelial cells in the relaxation of arterial smooth muscle by acetylcholine. *Nature* **288**: 373–376.
9. Banquet, S, Gomez, E, Nicol, L, Edwards-Lévy, F, Henry, JP, Cao, R *et al.* (2011). Arteriogenic therapy by intramyocardial sustained delivery of a novel growth factor combination prevents chronic heart failure. *Circulation* **124**: 1059–1069.
10. O'Shaugnessy, L (1937). Surgical treatment of cardiac ischemia. *Lancet* **232**: 185–194.
11. Takaba, K, Jiang, C, Nemoto, S, Saji, Y, Ikeda, T, Urayama, S *et al.* (2006). A combination of omental flap and growth factor therapy induces arteriogenesis and increases myocardial perfusion in chronic myocardial ischemia: evolving concept of biologic coronary artery bypass grafting. *J Thorac Cardiovasc Surg* **132**: 891–899.
12. Shrager, JB, Wain, JC, Wright, CD, Donahue, DM, Vlahakes, GJ, Moncure, AC *et al.* (2003). Omentum is highly effective in the management of complex cardiothoracic surgical problems. *J Thorac Cardiovasc Surg* **125**: 526–532.
13. Shudo, Y, Miyagawa, S, Fukushima, S, Saito, A, Shimizu, T, Okano, T *et al.* (2011). Novel regenerative therapy using cell-sheet covered with omentum flap delivers a huge number of cells in a porcine myocardial infarction model. *J Thorac Cardiovasc Surg* **142**: 1188–1196.
14. Kawamura, M, Miyagawa, S, Fukushima, S, Saito, A, Miki, K, Ito, E *et al.* (2013). Enhanced survival of transplanted human induced pluripotent stem cell-derived cardiomyocytes by the combination of cell sheets with the pedicled omental flap technique in a porcine heart. *Circulation* **128**(11 Suppl 1): S87–S94.
15. Mancuso, MR, Davis, R, Norberg, SM, O'Brien, S, Sennino, B, Nakahara, T *et al.* (2006). Rapid vascular regrowth in tumors after reversal of VEGF inhibition. *J Clin Invest* **116**: 2610–2621.
16. Inai, T, Mancuso, M, Hashizume, H, Baffert, F, Haskell, A, Baluk, P *et al.* (2004). Inhibition of vascular endothelial growth factor (VEGF) signaling in cancer causes loss of endothelial fenestrations, regression of tumor vessels, and appearance of basement membrane ghosts. *Am J Pathol* **165**: 35–52.
17. Shimizu, T, Sekine, H, Yang, J, Isoi, Y, Yamato, M, Kikuchi, A *et al.* (2006). Polysurgery of cell sheet grafts overcomes diffusion limits to produce thick, vascularized myocardial tissues. *FASEB J* **20**: 708–710.
18. Carmeliet, P and Conway, EM (2001). Growing better blood vessels. *Nat Biotechnol* **19**: 1019–1020.
19. Hagège, AA, Vilquin, JT, Bruneval, P and Menasché, P (2001). Regeneration of the myocardium: a new role in the treatment of ischemic heart disease? *Hypertension* **38**: 1413–1415.
20. Weis, SM and Cheresh, DA (2005). Pathophysiological consequences of VEGF-induced vascular permeability. *Nature* **437**: 497–504.
21. Cao, Y, Hong, A, Schulten, H and Post, MJ (2005). Update on therapeutic neovascularization. *Cardiovasc Res* **65**: 639–648.
22. Adams, RH and Alitalo, K (2007). Molecular regulation of angiogenesis and lymphangiogenesis. *Nat Rev Mol Cell Biol* **8**: 464–478.
23. Jenkins, MJ, Edgley, AJ, Sonobe, T, Umetani, K, Schwenke, DO, Fujii, Y *et al.* (2012). Dynamic synchrotron imaging of diabetic rat coronary microcirculation in vivo. *Arterioscler Thromb Vasc Biol* **32**: 370–377.
24. Iwasaki, H, Fukushima, K, Kawamoto, A, Umetani, K, Oyamada, A, Hayashi, S *et al.* (2007). Synchrotron radiation coronary microangiography for morphometric and physiological evaluation of myocardial neovascularization induced by endothelial progenitor cell transplantation. *Arterioscler Thromb Vasc Biol* **27**: 1326–1333.
25. Ludmer, PL, Selwyn, AP, Shook, TL, Wayne, RR, Mudge, GH, Alexander, RW *et al.* (1986). Paradoxical vasoconstriction induced by acetylcholine in atherosclerotic coronary arteries. *N Engl J Med* **315**: 1046–1051.
26. Marti, CN, Gheorghiade, M, Kalogeropoulos, AP, Georgiopoulou, VV, Quyyumi, AA and Butler, J (2012). Endothelial dysfunction, arterial stiffness, and heart failure. *J Am Coll Cardiol* **60**: 1455–1469.
27. Bonetti, PO, Lerman, LO and Lerman, A (2003). Endothelial dysfunction: a marker of atherosclerotic risk. *Arterioscler Thromb Vasc Biol* **23**: 168–175.
28. Poelzl, G, Frick, M, Huegel, H, Lackner, B, Alber, HF, Mair, J *et al.* (2005). Chronic heart failure is associated with vascular remodeling of the brachial artery. *Eur J Heart Fail* **7**: 43–48.
29. Meyer, B, Mörtl, D, Strecker, K, Hülsmann, M, Kulemann, V, Neunteufl, T *et al.* (2005). Flow-mediated vasodilation predicts outcome in patients with chronic heart failure: comparison with B-type natriuretic peptide. *J Am Coll Cardiol* **46**: 1011–1018.
30. Heitzer, T, Baldus, S, von Kodolitsch, Y, Rudolph, V and Meinertz, T (2005). Systemic endothelial dysfunction as an early predictor of adverse outcome in heart failure. *Arterioscler Thromb Vasc Biol* **25**: 1174–1179.

OPEN ACCESS Freely available online

PLOS | ONE

N-Glycans: Phenotypic Homology and Structural Differences between Myocardial Cells and Induced Pluripotent Stem Cell-Derived Cardiomyocytes

Takuji Kawamura[1], Shigeru Miyagawa[1], Satsuki Fukushima[1], Akira Yoshida[2], Noriyuki Kashiyama[1], Ai Kawamura[1], Emiko Ito[1], Atsuhiro Saito[1], Akira Maeda[3], Hiroshi Eguchi[3], Koichi Toda[1], Jong-Kook Lee[2], Shuji Miyagawa[3], Yoshiki Sawa[1]*

1 Department of Cardiovascular Surgery, Osaka University Graduate School of Medicine, Suita, Osaka, Japan, **2** Department of Cardiovascular Regenerative Medicine, Osaka University Graduate School of Medicine, Suita, Osaka, Japan, **3** Division of Organ Transplantation, Department of Surgery, Osaka University Graduate School of Medicine, Suita, Osaka, Japan

Abstract

Cell surface glycans vary widely, depending on cell properties. We hypothesized that glycan expression on induced pluripotent stem cells (iPSCs) might change during cardiomyogenic differentiation toward the myocardial phenotype. *N*-glycans were isolated from iPSCs, iPSC-derived cardiomyocytes (iPSC-CM), and original C57BL/6 mouse myocardium (Heart). Their structures were analyzed by a mapping technique based on HPLC elution times and MALDI-TOF/MS spectra. Sixty-eight different *N*-glycans were isolated; the structures of 60 of these *N*-glycans were identified. The quantity of high-mannose type (immature) *N*-glycans on the iPSCs decreased with cardiomyogenic differentiation, but did not reach the low levels observed in the heart. We observed a similar reduction in neutral *N*-glycans and an increase in fucosylated or sialyl *N*-glycans. Some structural differences were detected between iPSC-CM and Heart. No *N*-glycolyl neuraminic acid (NeuGc) structures were detected in iPSC-CM, whereas the heart contained numerous NeuGc structures, corresponding to the expression of cytidine monophosphate-*N*-acetylneuraminic acid hydroxylase. Furthermore, several glycans containing Galα1-6 Gal, rarely identified in the other cells, were detected in the iPSC-CM. The expression of *N*-glycan on murine iPSCs changed toward the myocardial phenotype during cardiomyogenic differentiation, leaving the structural differences of NeuGc content or Galα1-6 Gal structures. Further studies will be warranted to reveal the meaning of the difference of *N*-glycans between the iPSC-CM and the myocardium.

Citation: Kawamura T, Miyagawa S, Fukushima S, Yoshida A, Kashiyama N, et al. (2014) *N*-Glycans: Phenotypic Homology and Structural Differences between Myocardial Cells and Induced Pluripotent Stem Cell-Derived Cardiomyocytes. PLoS ONE 9(10): e111064. doi:10.1371/journal.pone.0111064

Editor: Toru Hosoda, Tokai University, Japan

Received April 30, 2014; **Accepted** September 19, 2014; **Published** October 30, 2014

Data Availability: The authors confirm that all data underlying the findings are fully available without restriction. All relevant data are within the paper and its Supporting Information files.

Funding: YS received the funding to support this work from the Research Center Network for Realization of Regenerative Medicine managed by Centers for Clinical Application Research on Specific Disease/Organ and funded by Japan Science and Technology Agency. The funders had no role in study design, data collection and analysis, decision to publish, or preparation of the manuscript.

Competing Interests: The authors have declared that no competing interests exist.

* Email: sawa-p@surg1.med.osaka-u.ac.jp

Introduction

In vitro generation of cardiac myocytes by reprogramming is a promising technology in developing cell-transplant therapy for advanced cardiac failure [1] and drug discovery for a variety of cardiac diseases [2]. For both purposes, induced pluripotent stem cells (iPSCs) are most useful, since generation and cardiomyogenic differentiation of iPSCs has been standardized in human and a number of animals [3,4]. In fact, derivatives of iPSCs have been developed to the pre-clinical stage for cell transplantation therapy [5], while cardiac myocytes generated from patient-specific iPSCs have been studied to explore pathologic mechanisms and guide drug discovery [6,7]. However, cardiac myocyte preparations from iPSCs contain immature phenotypes, observed by electrophysiology, electron microscopy, and immunohistochemistry [8,9]; this may limit the safety and efficacy of cell transplantation therapy or reduce the accuracy and efficiency of drug discovery. The maturity of iPSC-derived cardiac myocytes (iPSC-CMs) has not been comprehensively or quantitatively evaluated.

Cell surface glycans have several important functions interacting with numerous proteins, including growth factors, morphogens and adhesion molecules, modulating dynamic cellular mechanisms such as cell-cell adhesion, cell activation, and malignant alterations [10–12]. In early mammalian embryos, associated with fertilization, some *N*-glycans play important roles of cell-cell adhesion [13–15]. In addition, cellular responsiveness to growth or arrest depends on total *N*-glycan number and the degree of branching of cell surface glycoproteins [16]. Furthermore, heparan sulfate, a kind of glycans, is required for embryonic stem cell (ESC) pluripotency, in particular lineage specification into mesoderm through facilitation of FGF and BMP signaling by stabilizing BMP ligand [17], leading the evidence that the expression patterns of cell surface glycans on ESCs changes during differentiation [18]. Thus, we hypothesized that cell surface glycan expression may

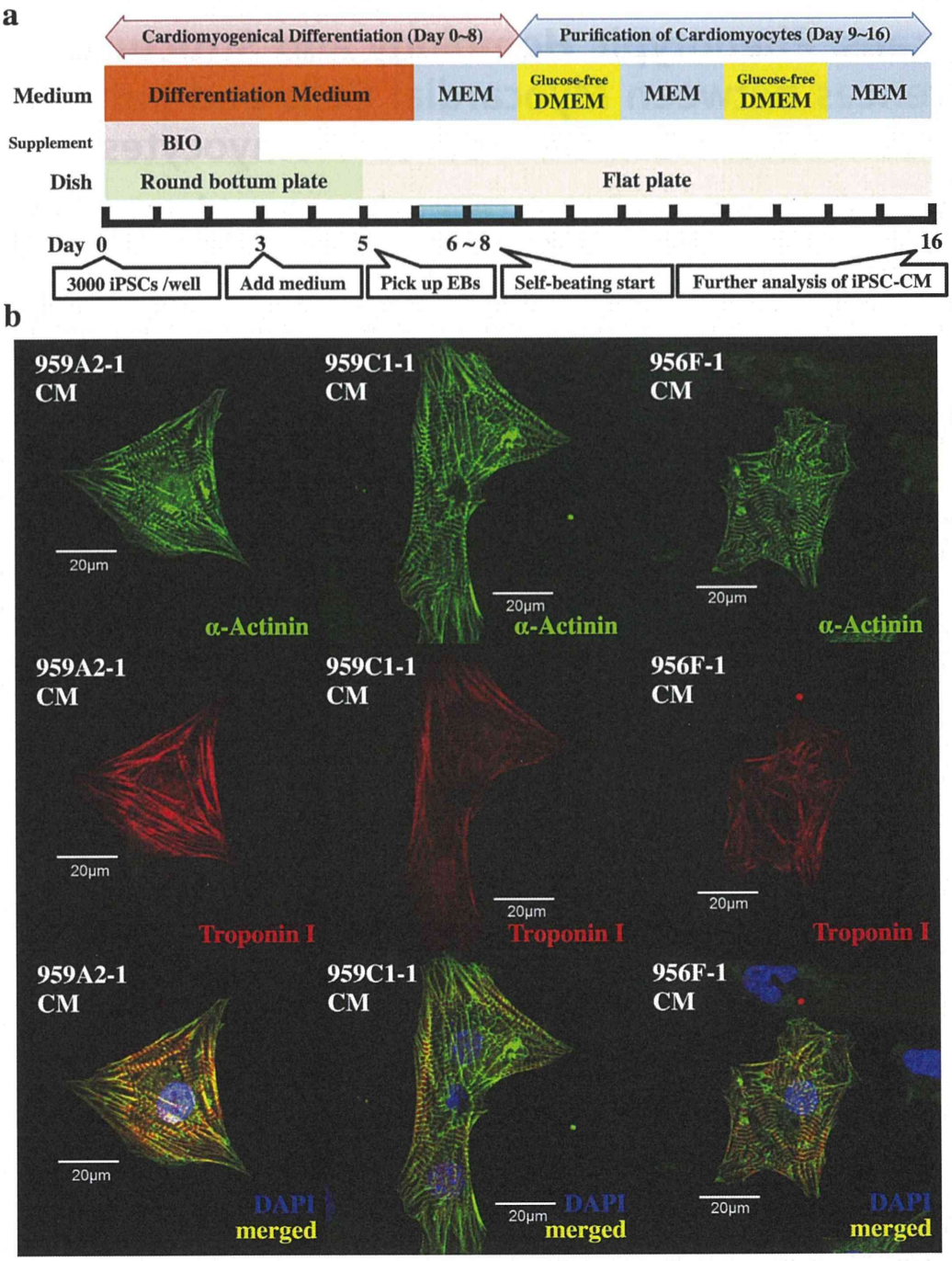

Figure 1. Cardiomyogenic differentiation of iPSCs and cardiomyocyte purification. (a) The cardiomyogenic differentiation protocol and cardiomyocyte purification process are illustrated. (b) IPSC-CMs stained with anti-α-actinin antibody (Alexa Fluor 488), anti-troponin I (Alexa Fluor 594) and DAPI, were analyzed with a confocal laser scanning microscopy. Abbreviations: EB, embryonic body; MEM, Modified Eagle's Medium; DMEM, Dulbecco's Modified Eagle's Medium; BIO, 6-bromoindirubin-3′-oxime.
doi:10.1371/journal.pone.0111064.g001

change during the course of cardiomyogenic differentiation of iPSCs *in vitro*. We analyzed *N*-glycan expression in undifferentiated iPSCs, iPSC-CMs, and adult murine myocardium by HPLC, to identify potential indicators of the maturity of differentiating cardiomyocytes from iPS cells *in vitro*.

Materials and Methods

Animal care procedures were consistent with the "Guide for the Care and Use of Laboratory Animals" (National Institutes of Health publication). Experimental protocols were approved by the

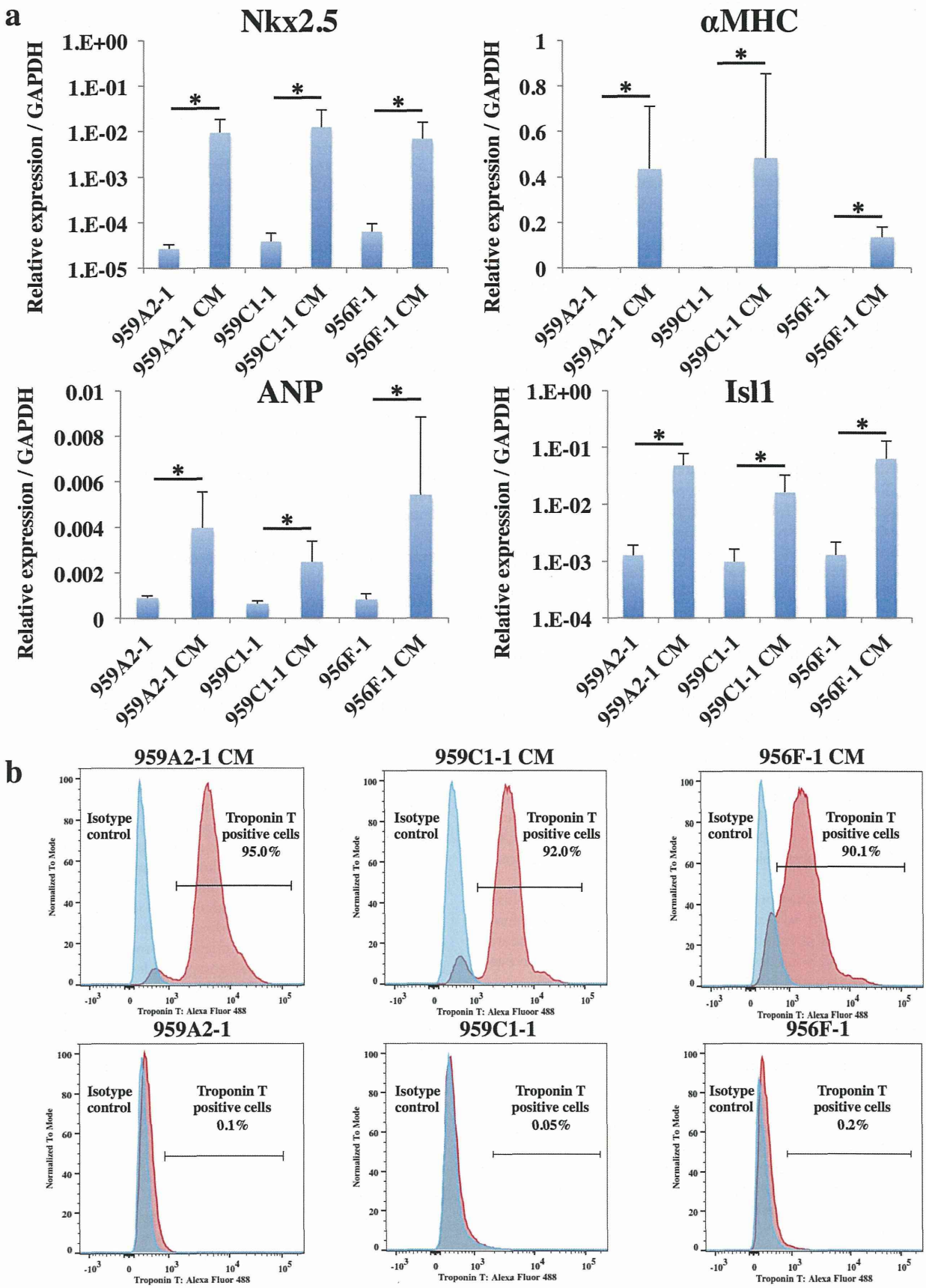
a
Nkx2.5
Relative expression / GAPDH
1.E+00
1.E-01
1.E-02
1.E-03
1.E-04
1.E-05
αMHC
1
0.8
0.6
0.4
0.2
0
ANP
0.01
0.008
0.006
0.004
0.002
0
Isl1
959A2-1
959A2-1 CM
959C1-1
959C1-1 CM
956F-1
956F-1 CM
b
959A2-1 CM
959C1-1 CM
956F-1 CM
Isotype control
Troponin T positive cells 95.0%
Troponin T positive cells 92.0%
Troponin T positive cells 90.1%
959A2-1
959C1-1
956F-1
Troponin T positive cells 0.1%
Troponin T positive cells 0.05%
Troponin T positive cells 0.2%
Normalized To Mode
Troponin T: Alexa Fluor 488

Figure 2. Highly purified iPSC-CMs expressing cardiomyocyte marker genes. (a) Transcript expression of Nkx2.5, αMHC, ANP and Isl1 in the iPSCs and the iPSC-CMs were analyzed by real-time PCR. Results are expressed as the mean ± standard deviation. *P<0.05. (b) IPSC-CMs and iPSCs stained with anti-troponin T antibody or the isotype control, followed by Alexa Fluor 488-conjugated anti-mouse IgG antibody, were analyzed by flow cytometry.
doi:10.1371/journal.pone.0111064.g002

Ethics Review Committee for Animal Experimentation of Osaka University Graduate School of Medicine.

Cardiomyogenic differentiation of murine iPSCs *in vitro*

We used the murine iPSC lines, 959A2-1, 959C1-1, 956F-1 (generous gifts from Dr. Okita and Professor Yamanaka of the Center for iPS Cell Research and Application, Kyoto University, Kyoto, Japan). The cell lines were generated from C57BL/6 (B6) (CLEA) mouse embryonic fibroblasts by introducing *Oct3/4, Sox2, Klf4*, and *c-Myc* without viral vectors as described [19]. The iPSCs were cultured in the absence of serum and feeder cells by using ESGRO Complete PLUS Clonal Grade Medium (Millipore).

Cardiomyogenic differentiation of the iPSCs was performed as described [20,21], with modifications, followed by purification with glucose-free medium supplemented with lactic acid [22]; iPSCs (3×10^3) were resuspended in 100-μL aliquots of differentiation medium [DM; Dulbecco's Modified Eagle's Medium (DMEM; Nacalai Tesque) containing 15% fetal bovine serum (FBS; Biofill), 100 μmol/L non-essential amino acids (NEAA; Invitrogen), 2 mmol/L L-glutamine (Invitrogen), and 0.1 mmol/L 2-mercaptoethanol (Invitrogen)] containing 0.2 μmol/L 6-bromoindirubin-3′-oxime (BIO; a glycogen synthase kinase-3β inhibitor, to activate the Wnt-signaling pathway) (Calbiochem), and cultured in 96-well Corning Costar Ultra-Low attachment multiwell plates (Sigma-Aldrich) for 3 days. On day 3, an additional 100 μL DM without BIO was added to each well. On day 5, individual embryoid bodies (EBs) were transferred to 100-mm gelatin-coated dishes (250 EBs per dish). On days 6, 7, 10, 11, 14, and 15 the medium was exchanged for serum-free Modified Eagle's Medium (MEM; Invitrogen) with insulin transferrin-selenium-X (Invitrogen). On days 8, 9, 12, and 13, the medium was exchanged for Glucose-free DMEM (no glucose, no pyruvate, Invitrogen) supplemented with 4 mmol/L lactic acid (Wako Pure Chemical) for purification of cardiomyocytes. On day 16, the contracting cell clusters were used as cardiomyogenically differentiated iPSCs (959A2-1 CMs, 959C1-1 CMs, 956F-1 CMs: iPSC-CMs). The protocol and purification process are illustrated in Figure 1a.

Adult cardiac tissue from B6 mice (CLEA) was used as a control. Male B6 mice (8 weeks old) were sacrificed by intravenous administration of potassium chloride under inhalation anesthesia of isoflurane, and heart tissue from the left ventricle was harvested for further studies and labeled "Heart".

Immunohistochemistry analysis

IPSC-CMs were dissociated with 0.25% trypsin-EDTA and then fixed with 4% paraformaldehyde. The cells were stained with the following primary antibodies: mouse anti-α-actinin antibody (Sigma-Aldrich) and rabbit anti-troponin I antibody (Abcam), and then visualized by the following secondary antibodies: Alexa Fluor 488 donkey anti-mouse IgG (Invitrogen) and Alexa Fluor 594 goat anti-rabbit IgG (Invitrogen). The nucleus of the cells were stained with 4′, 6-Diamidino-2-phenylindole dihydrochloride (DAPI) and then observed with a confocal laser scanning microscopy FV1200 (Olympus).

Ca^{2+} transient measurement and pharmacological analysis

5 μM Fluo-8 regents (AAT Bioquest, Inc.) in serum-free MEM was added to iPSC-CMs after the cells were washed with phosphate buffered saline. The cells were incubated at 37°C for 30 min and then observed with a fluorescence microscopy. Fluorescence intensity of Fluo-8 dye was sequentially measured using iQ2 software (ANDOR) pre and post the administration of 1 μM isoproterenol.

Flow cytometry

IPSC-CMs were dissociated with 0.25% trypsin-EDTA and then fixed with CytoFix fixation buffer (BD) for 20 min. The cells were permeabilized with Perm/Wash buffer (BD) at room temperature for 10 min and then incubated with mouse anti-troponin T antibody (Thermo) for 30 min. Cells were washed with Perm/Wash buffer prior to incubation with the Alexa Fluor 488 rabbit anti-mouse IgG secondary antibody (Invitrogen) at room temperature for 30 min. These cells were analyzed on a FACS Canto II (BD).

Characterization of *N*-glycans derived from iPSCs, iPSC-CM, and Heart

All experimental procedures, including chromatography conditions and glycosidase treatments, have been described previously [23]. Cultured undifferentiated iPSCs, iPSC-CMs, and the heart tissue were treated with chloroform–methanol, then subjected to proteolysis with chymotrypsin and trypsin, followed by glycoamidase A digestion to release *N*-glycans. After removal of peptides, the reducing ends of the *N*-glycans were derivatized with 2-aminopyridine (Wako). This mixture was applied to a diethylaminoethyl (DEAE) column (Tosoh) or a TSK-gel Amide-80 column (Tosoh); each fraction from the amide column was then applied to a Shim-pack HRC-octadecyl silane (ODS) column (Shimadzu). The elution times of individual peaks from the amide-silica and ODS columns were normalized to a pyridylamino (PA)-derivatized isomalto-oligosaccharide with a known degree of polymerization, and are represented as glucose units (GU). Thus, each compound from these two columns provided a unique set of GU values, which corresponded to the coordinates of the 2D HPLC map. The PA-oligosaccharides were identified by comparison to the coordinates of ~500 reference PA-oligosaccharides in a homemade web application, GALAXY (http://www.glycoanalysis.info/galaxy2/ENG/index.jsp) [24]. The calculated HPLC map based on the unit contribution values was used to estimate some high-mannose type PA-oligosaccharides. The PA-oligosaccharides were co-chromatographed with the reference to PA-oligosaccharides on the columns to confirm their identities. PA-glycans that did not correspond to any of the *N*-glycans registered in GALAXY were trimmed by exoglycosidase to produce a series of known glycans [25].

Mass spectrometry

PA-oligosaccharides were analyzed by matrix-assisted laser desorption/ionization time-of-flight mass spectrometric (MALDI-TOF/MS). The matrix solution was prepared as follows: 10 mg of 2,5-Dihydroxybenzoic acid (Sigma) was dissolved in 1:1 (v/v)

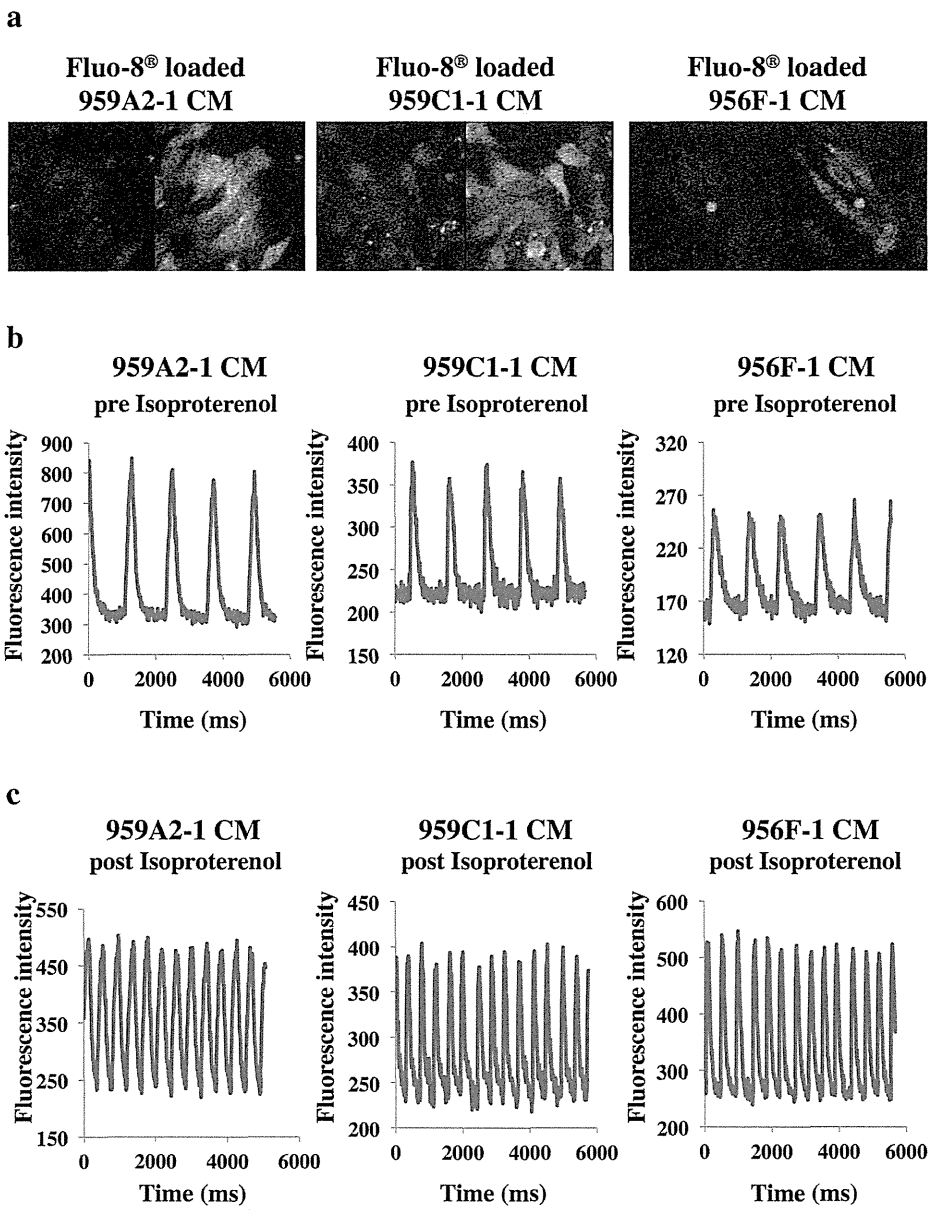

Figure 3. Ca^{2+} transient measurement of iPSC-CMs pre and post the administration of isoproterenol. (a) Fluo-8 loaded iPSC-CMs at the time of low (left) and high (right) fluorescence. (b), (c) Sequentially measured fluorescence intensity of Fluo-8 loaded iPSC-CMs pre (b) and post (c) the administration of 1 μM isoproterenol.
doi:10.1371/journal.pone.0111064.g003

acetonitrile/water (1 mL). Stock solutions of PA-glycans were prepared by dissolving them in pure water. One microliter of a sample solution was mixed on the target spot of a plate with 1 μL matrix solution and then allowed to air-dry. MALDI-TOF/MS data were acquired in the positive mode on an AXIMA-CFR (Shimadzu) operated in linear mode.

Materials

Glycoamidase A from sweet almond, α-mannosidase, β-galactosidase, and β-*N*-acetylhexosaminidase from jack bean were purchased from Seikagaku Kogyo (Tokyo, Japan). α-Galactosidase from coffee bean was purchased from Oxford GlycoSciences (Oxford, UK). Trypsin and chymotrypsin were obtained from Sigma (St. Louis, MO). Pronase protease from *Streptomyces griseus* was from Calbiochem (San Diego, CA). The pyridylamino (PA) derivatives of isomalto-oligosaccharides 4–20 (indicating the degree of polymerization of glucose residues) and reference PA-oligosaccharides were purchased from Seikagaku Kogyo.

Semi-quantitative PCR

DNA-free total RNA was extracted with the RNeasy RNA isolation Kit (Qiagen) and reverse-transcribed into cDNA using Omniscript reverse transcriptase (Qiagen), then analyzed by quantitative real-time PCR on an ABI PRISM 7700 thermocycler (Applied Biosystems) with the following TaqMan gene expression assays (Applied Biosystems): ST3Gal-III (Gal β1-3(4) GlcNAc α-2,

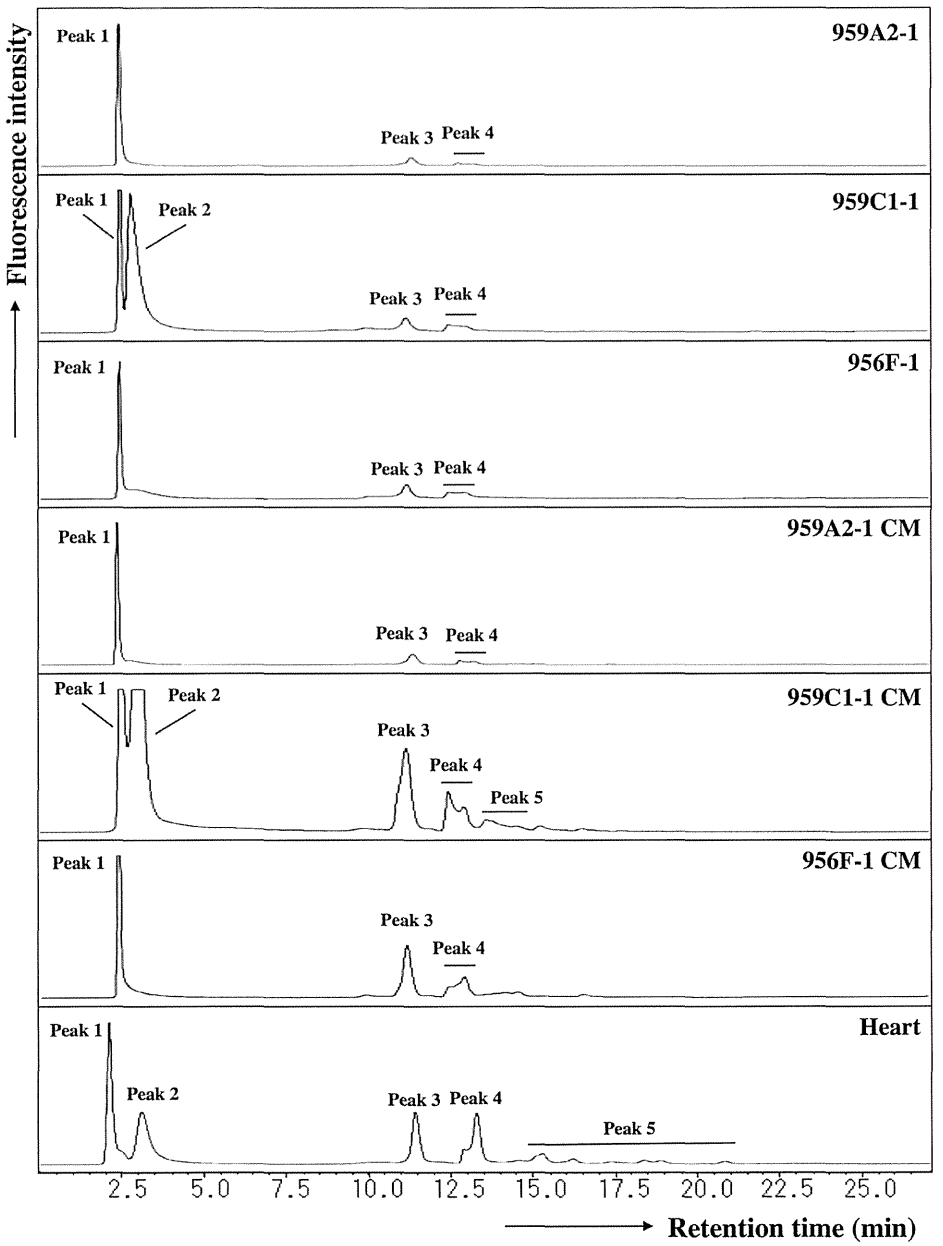

Figure 4. Anion-exchange DEAE elution profiles of PA-glycans. PA-glycans were fractionated according to their sialic acid content as neutral (peak 1), monosialyl (peak 3), and disialyl (peak 4) oligosaccharide fractions. Peaks 2 and 5 represent fractions containing no detectable PA-oligosaccharides.
doi:10.1371/journal.pone.0111064.g004

3-sialyltransferase), Mm00493353_m1; ST4Gal-IV (Gal β1-4(3) GlcNAc α-2, 3-sialyltransferase), Mm00501503_m1; ST6Gal-I (Gal β1-4 GlcNAc α-2, 6-sialyltransferase), Mm00486119_m1; CMAH (cytidine monophosphate-*N*-acetylneuraminic acid hydroxylase), Mm00483341_m1; GAPDH (glyceraldehyde-3-phosphate dehydrogenase), and Mm03302249_g1 and with SYBR Green dye (Applied Biosystems) using the following primers: Nkx2.5 F, 5′- CAAGTGCTCTCCTGCTTTCC -3′ R, 5′- GGCTTTGTCCAGCTCCACT -3′; αMHC (α-myosin heavy chain) F, 5′- GAGATTTCTCCAACCCAG -3′ R, 5′- TCTGACTTTCGGAGGTACT-3′; ANP (atrial natriuretic peptide) F, 5′- AAAGAAACCAGAGTGGGCAGAG -3′ R, 5′- CCAGGGTGATGGAGAAGGAG -3′; Isl1 F, 5′- TTTCCCTGTGTGTTGGTTGC -3′ R, 5′- TGATTACACTCCGCACATTTCA -3′; GAPDH F, 5′- CCAGTATGACTCCACTCACG -3′ R, 5′- GACTCCACGACATACTCAGC -3′. All experiments were performed by the relative standard curve method in three independent, triplicate experiments. Statistical comparison of the data was performed by Student's t-test.

Results

Highly purified cardiomyocytes derived from iPSCs

Cardiomyogenic differentiation was induced in murine iPSCs by using a slightly modified culture protocol (Figure 1a). The iPSC-CMs showed significantly higher expressions of Nkx2.5,

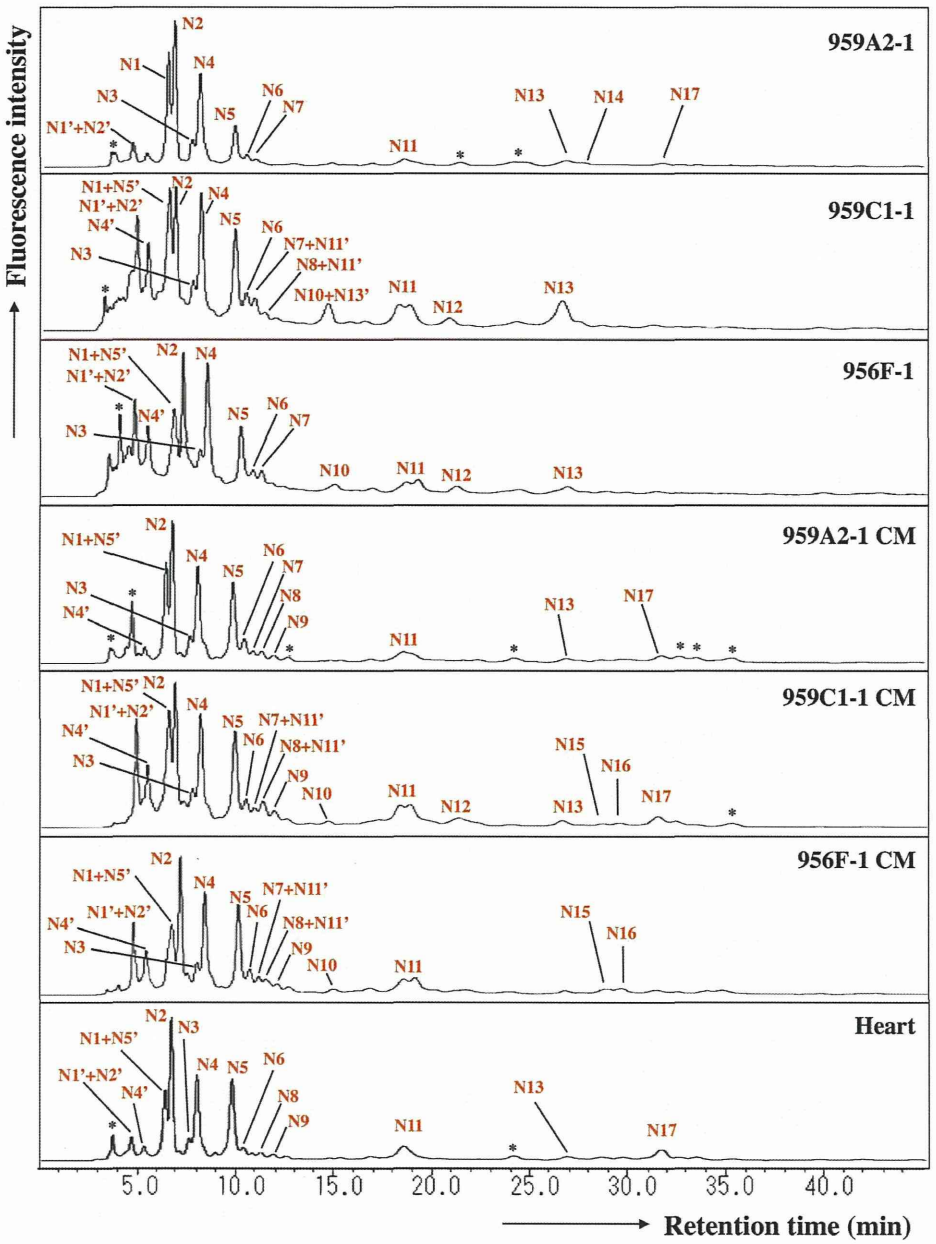

Figure 5. Reverse-phase ODS elution profiles of the neutral PA-glycans. The neutral fractions were individually applied to the ODS column and eluted according to their hydrophobicity. N1′, N2′, N4′, N5′ and N11′: epimerization of N1, N2, N4, N5 and N11. *Fractions containing no detectable PA-oligosaccharides.
doi:10.1371/journal.pone.0111064.g005

αMHC, ANP and Isl1 than undifferentiated iPSCs by semi-quantitative real-time PCR (Figure 2a), and showed sarcomere structures observed by immunohistological staining of α-actinin and troponin I (Figure 1b). The iPSC-CMs were functional with Ca^{2+} transient measurement (Figure 3a, b) and their beating rates were increased by the administration of isoproterenol (Figure 3c), meaning they had β-adrenergic receptors. Nearly all of the iPSC-CMs exhibited spontaneous and regular beating at room temperature (Video S1). The differentiation efficiency of murine iPSC was evaluated by flow cytometry analysis. More than 95% of the 959A2-1 CMs, 92% of the 959C1-1 CMs and 90% of the 956F-1 CMs were positive for troponin T (Figure 2b), while the undifferentiated iPSCs rarely expressed troponin T (Figure 2b).

N-Glycans isolated from iPSCs, iPSC-CM, and Heart

N-glycans extracted from undifferentiated iPSCs (959A2-1: 26 mg, 959C1-1: 11 mg and 956F-1: 10 mg of protein), iPSC-CM (959A2-1 CM: 15 mg, 959C1-1 CM: 12 mg and 956F-1 CM: 5.5 mg of protein), and the B6 heart muscle (82 mg of protein) were separated on a diethylaminoethyl (DEAE) column into five peaks, based on increasing acidity. Peak 1 represented a neutral (N) fraction, peak 3 a monosialyl (M) fraction, and peak 4 a disialyl

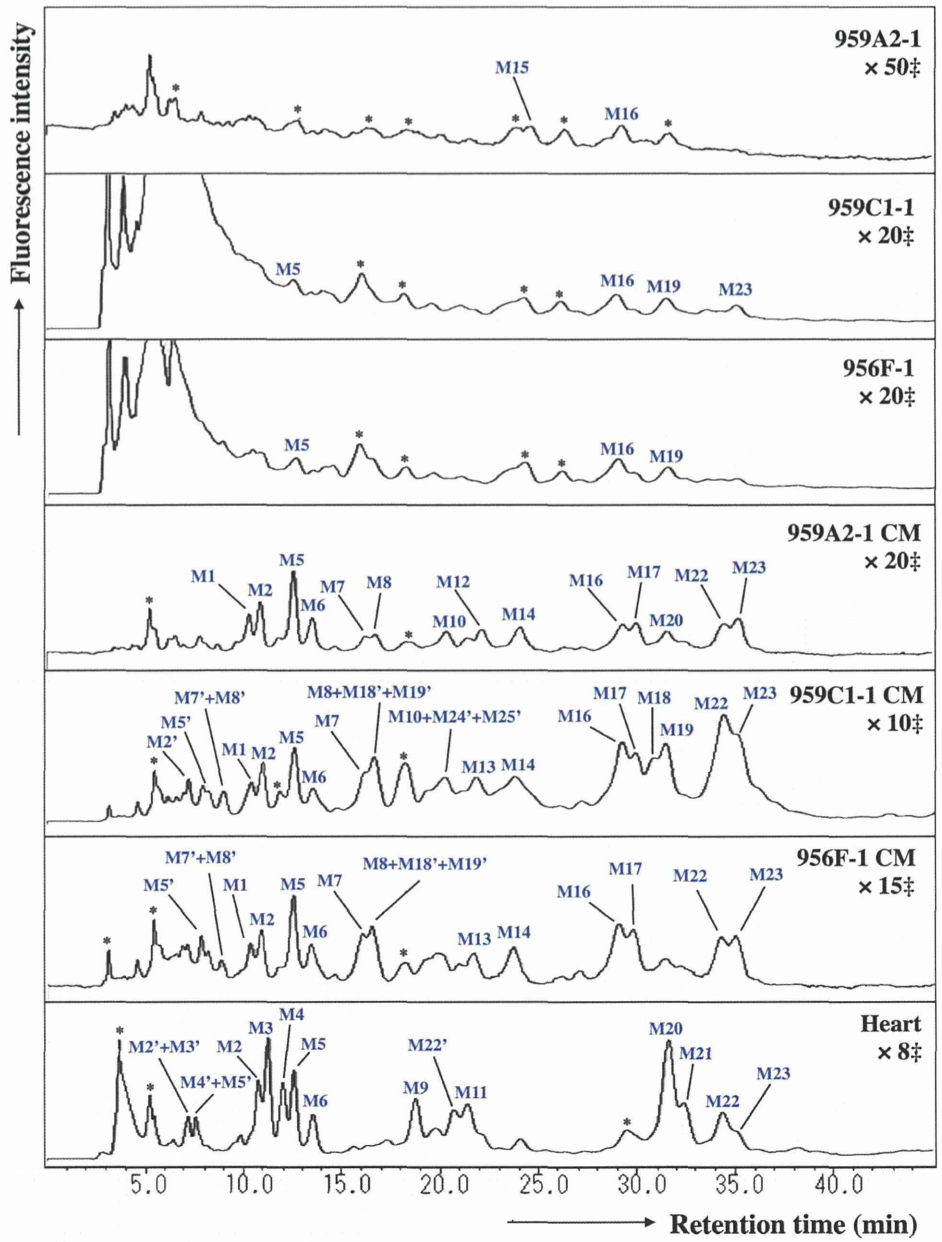

Figure 6. Reverse-phase ODS elution profiles of monosialyl PA-glycans. The monosialyl fractions were individually applied to the ODS column and eluted according to their hydrophobicity. M2′, M3′, M4′, M5′, M7′, M8′, M18′, M19′, M22′, M24′ and M25′: epimerization of M2, M3, M4, M5, M7, M8, M18, M19, M22, M24 and M25. *Fractions containing no detectable PA-oligosaccharides. ‡Magnification ratio to the fluorescence intensity of asialoglycan of each sample.
doi:10.1371/journal.pone.0111064.g006

(D) fraction. Glycan fractions in each of these peaks were as follows: iPSCs yielded 97% N, 0.5% M, 2.6% D (959A2-1), 98% N, 0.7% M, 1.1% D (959C1-1) and 96% N, 1.1% M, 3.1% D (956F-1) peak areas, iPSC-CMs yielded 89% N, 6.4% M, 4.4% D (959A2-1 CM), 79% N, 16% M, 4.8% D (959C1-1 CM) and 82% N, 10% M, 7.9% D (956F-1 CM) and Heart yielded 55% N, 19% M, and 25% D (Figure 4).

The ODS column separated the neutral fraction (Peak 1) into fractions N1–N17 (Figure 5), the monosialyl fraction (Peak 3) into fractions M1–M23 (Figure 6), and the disialyl fraction (Peak 4) into fractions D1–D12 (Figure 7). The signatures of each fraction differed between groups. These ODS fractions were individually fractionated on an amide column and analyzed by MALDI-TOF/MS. The N2, M6, M11, M14, M20, D4, D5, and D10 fractions contained two types of *N*-glycans, and the N6, N9, N11 and M2 fractions three types (data not shown). Thus, 68 different *N*-glycans were isolated from iPSCs, iPSC-CMs, and Heart.

Structures of *N*-Glycans isolated from iPSCs, iPSC-CM, and Heart

The isolated *N*-glycans were analyzed by means of a mapping technique based on their HPLC elution positions and MALDI-TOF/